JOURNAL OF MATERIALS SCIENCE: MATERIALS IN MEDICINE **10** (1999) 35–46

Surface characterization of implant materials c.p. Ti, Ti–6Al–7Nb and Ti–6Al–4V with different pretreatments

C. SITTIG, M. TEXTOR, N. D. SPENCER*
Laboratory for Surface Science and Technology, Department of Materials, ETH Zürich, Sonneggstr. 5, CH-8092 Zürich, Switzerland

M. WIELAND
Swiss Federal Laboratories for Materials Testing and Research, Überlandstr. 129, CH-8600 Dübendorf, Switzerland

P. -H. VALLOTTON
Institut Straumann AG, CH-4437 Waldenburg, Switzerland

The biocompatibility of commercially pure titanium and its alloys is closely related to their surface properties, with both the composition of the protecting oxide film and the surface topography playing an important role. Surfaces of commercially pure titanium and of the two alloys Ti–6Al–7Nb and Ti–6Al–4V (wt %) have been investigated following three different pretreatments: polishing, nitric acid passivation and pickling in nitric acid–hydrogen fluoride. Nitric acid treatment is found to substantially reduce the concentration of surface contaminants present after polishing. The natural 4–6 nm thick oxide layer on commercially pure titanium is composed of titanium oxide in different oxidation states (TiO_2, Ti_2O_3 and TiO), while for the alloys, aluminium and niobium or vanadium are additionally present in oxidized form (Al_2O_3, Nb_2O_5 or V-oxides). The concentrations of the alloying elements at the surface are shown to be strongly dependent on the pretreatment process. While pickling increases the surface roughness of both commercially pure titanium and the alloys, different mechanisms appear to be involved. In the case of commercially pure titanium, the dissolution rate depends on grain orientation, whereas in the case of the two alloys, selective α-phase dissolution and enrichment of the β-phase appears to occur.

1. Introduction

Titanium and its alloys, Ti–6Al–7Nb and Ti–6Al–4V (wt %), are among the most commonly used implant materials [1–3], particularly for dental, orthopaedic and osteosynthesis applications. These materials are known to have a combination of properties making them particularly suited for biomedical applications: passive surfaces promoting excellent corrosion resistance and low rates of metal ion release [1, 4–6], low specific weight, good overall mechanical properties, and little or no tendency to cause adverse cell or tissue reactions.

The interaction of the implant with its biological environment, the formation of a foreign material–tissue interface and the long-term success or failure of the integration in the body is now realized to be strongly connected with the surface properties of the implant device [7, 8]. Even within one type of material, such as commercially pure (c.p.) titanium, the degree of integration depends on the quality of the surface. There is strong interest, both from academic and industrial points of view, to better understand and exploit those surface properties that direct biological response. Several aspects of the titanium surface have been reported or suspected to influence the body response:

1. composition and structure of the oxide film,
2. surface contamination, and
3. surface topography.

The presence of a typically 4–6 nm thick titanium oxide (TiO_2) film that forms spontaneously when the surface is exposed to air or water [9] is responsible for the excellent corrosion resistance [10]. The surface chemistry might also influence other properties, such as the adsorption of specific cell-binding proteins,

* Author to whom correspondence should be addressed.

which is believed to depend both on the surface energy and on the sign and density of the surface charges [11, 12]. On the other hand, both the composition of the alloy and the manufacturing processes (thermal, mechanical and chemical treatments) influence the composition and the structure of the oxide film and therefore play an important role in biocompatibility properties.

Surface contamination is believed to be important [3, 13], because a fresh titanium oxide surface is very reactive towards both inorganic and organic contaminants. In an investigation of non-osseointegrated dental implants [14], contaminants such as Fe, Zn, Sn or Pb have been found on the implant surface and are believed to have contributed to the observed lack of osseointegration. On the other hand, the effects of elements such as C, H, N and O on the biological response are not well known. It has not been clearly established how surface treatment processes influence the type and degree of surface contamination on titanium.

Surface roughness has been reported [15–17] to determine the shear strength of the implant–bone interface–important for the long-term fixation. But also on the cell level, surface topography is known to influence cell adhesion, morphology, proliferation and differentiation [18–21] and therefore has a major influence on the evolution and the properties of the implant–tissue interface.

A collection of surface treatment processes are used today on an industrial scale to achieve desired surface properties such as cleanliness, passivation and specific topography. Polishing is often used on dental implants, to enhance gingival attachment, for example; nitric acid treatment homogenizes the passive film; anodization produces thick and dense oxide films; etching, particle blasting and plasma spraying of titanium are known to provide rough and/or porous surfaces suitable for osseointegration [17, 20–23]. Pickling of titanium is a well known process that both cleans and structures the surface [24].

Detailed information is missing, however, as regards all relevant surface aspects, namely oxide film composition, surface cleanliness and topography, and their dependence on alloy composition and surface treatment parameters. The present work aims at filling this gap by providing statistically significant data on the materials c.p. Ti, Ti–6Al–7Nb and Ti–6Al–4V after different surface treatments, i.e. mechanical polishing, passivation in nitric acid, and pickling in nitric acid–hydrofluoric acid solution. The compositions and thicknesses of the oxide films were determined by X-ray photoelectron spectroscopy (XPS). Laser profilometry (LPM) and scanning electron microscopy (SEM) were used to evaluate surface topography. Additionally, the effect of γ-sterilization on the surface composition was investigated.

2. Experimental procedure

2.1. Bulk analysis and sample fabrication

Both c.p. Ti and Ti–6Al–7Nb samples consisted of 15 mm diameter, 1 mm thick discs. A stamping procedure was used to produce the Ti discs out of a Grade 2 c.p. Ti sheet (ASTM F67) in an annealed condition, whereas Ti–6Al–7Nb discs were turned and trued from a 20 mm diameter rod. Ti–6Al–4V samples were obtained from 3 mm thick discs, cut from a 22 mm rod and subsequently divided into four parts. Laboratory analyses of the three materials used in this study are given in Table I.

TABLE I Laboratory analysis of c.p. Ti, Ti–6Al–7Nb and Ti–6Al–4V samples used in this study

Element (%)	c.p. Ti	Ti–6Al–7Nb	Ti–6Al–4V
Al	0.0055	6.035	6.095
Nb	–	7.03	–
V	< 0.03	–	3.815
O	0.14	0.16	0.04
N	0.01	0.01	< 0.01
H[a]	13	51	53
C	0.002	0.007	0.004
Cu	0.0015	< 0.02	< 0.02
Ni	0.008	0.017	0.013
Mn	0.006	0.001	0.0055
Fe	0.0245	0.15	0.06
Zr	< 0.005	< 0.02	< 0.02
Mo	< 0.005	< 0.02	< 0.02
Cr	< 0.005	–	–
W	< 0.01	< 0.03	< 0.03
Sn	0.0105	< 0.02	< 0.02

[a] H is measured in milligrams per gram.

2.2. Surface preparation

Mechanically polished samples were prepared by using SiC grinding paper (ultimate grit size 600–15 μm particle diameter), subsequently polished to a mirror finish with 10 μm diamond paste in oil and finally with a 0.06 μm SiO_2 suspension. Immediately after polishing, the following surface-cleaning procedure was used: degreasing in ethanol, rinsing in running deionized water, immersing in a HNO_3 30 vol % solution for 1 min with ultrasonic agitation, neutralizing and rinsing in running deionized water, and eventually drying with hot air.

The passivated samples were polished, then passivated in 30 vol % HNO_3 for 15 min at room temperature and finally rinsed in deionized water and dried with hot air.

To investigate the effect of pickling, samples with four different starting surfaces (polished, cold-worked and annealed, turned, cut) were pickled. Prior to treatment, the samples were degreased for 3 min at pH 12 in a commonly used cleaning solution (Deconex 15PF, Merck) with ultrasonic agitation, then rinsed in hot running water and finally in deionized running water. Pickling was performed in a solution of 0.18 M HF and 1.88 M HNO_3 in deionized water at 20 °C, using different times, with and without ultrasonic agitation. Samples were then rinsed and neutralized in deionized water and dried with hot air.

All samples were wrapped in aluminium foil for storage until they were introduced into the ultra-high vacuum (UHV) system of the XPS instrument.

TABLE II Number of investigated samples (materials, surfaces and treatments) characterized by XPS (X), LPM (L) and SEM (S)

	As-polished	Passivated	Pickled				As-polished and sterilized	Passivated and sterilized	Pickled and sterilized
			For 3 min[a]	For 3 min	For 10 min[a]	For 10 min[a]			For 3 min[a]
C.p. Ti			5X						
Cold-worked + annealed			2×3^b L 1S	2×3^b L					
	5X	5X							
Polished	3×2^b L 1S	3×2^b L 1S	2×3^b L 1S	2×3^b L	2×3^b L 1S				
Ti–Al–Nb						5X			
Turned						2×3^b L 1S			
	5X	5X					5X	5X	5X
Polished	3×2^b L 1S	3×2^b L 1S			2×3^b L 1S				
Ti–Al–V					5X				
Cut					2×3^b L 1S				
	5X	5X							
Polished	3×2^b L 1S	3×2^b L 1S			2×3^b L 1S				

[a] Samples subjected to ultrasonic treatment during pickling
[b] Two samples were characterized with three lines per sample.

Selected samples were submitted to a γ-sterilization treatment (30 kGy) corresponding to that used for dental implants.

Table II lists all materials and surface treatment types investigated in this study.

2.3. Surface characterization

Standard metallography techniques were used in order to characterize the microstructure of the three materials used in this study.

The topography of the sample surfaces after the different pretreatments was investigated by SEM using a Jeol 840 A. On the alloy surfaces, areas with different elemental composition were detected in composition contrast mode (from backscattered electrons) and specifically analysed using energy dispersive X-ray analysis (EDX) (Tracor Northen TN 5400).

Roughness values were measured with a non-contact laser profilometer developed by UBM, Ettlingen, Germany. The lateral resolution of this method is given by the size of the focused laser beam, which is approximately 1 μm for the instrument used, and the z-resolution is about 0.01 μm. Line scans were taken over a length of 1.75 mm with 1400 points mm^{-1} for the polished surfaces and 5.6 mm with 500 points mm^{-1} for the pickled surfaces. The roughness value, R_a (arithmetic average of the absolute values of all points of the profile), $R_{z_{ISO}}$ (arithmetic average of the five highest profile peaks and five lowest profile valleys over the entire measured trace) and N_r (standardized peak count on a profile length of 10 mm) were calculated using the software provided by UBM. In the calculation of the roughness values, the cut-off was set at 0.25 mm for the polished surfaces and to 0.8 mm for the pickled surfaces.

XPS spectra were recorded with a Specs SAGE 100 system using unmonochromatized MgK_α radiation at 300 W (12 kV). The instrumental vacuum was 2.5×10^{-8} mbar. Measurements were made at a take-off angle of 90° with respect to the surface of the sample. The area of information is typically 9×9 mm^2 and the results therefore represent laterally averaged chemical composition. Survey scans over a binding energy range of 0–1150 eV were taken for each sample with a constant detector pass energy of 50 eV, followed by high-resolution spectra with a detector pass energy of 14 eV. The line width of the Ag (3d5/2) signal in the high-resolution mode is typically < 1 eV with a height of $> 120\,000$ counts s^{-1}.

The high-resolution XPS measurements allow the determination of the oxidation state of elements and of the oxide-layer thickness. Background subtraction (Shirley or linear type), peak integration and/or fitting were carried out using the SpecsLab software. To determine surface composition from XPS data, the sensitivity factors of Evans *et al.* [25] were used. Small concentrations of V are difficult to detect with unmonochromatized excitation radiation, due to the nearby O (1s) satellites; therefore the Ti–6Al–4V samples were investigated with monochromatized AlK_α radiation (XPS, PHI 5700), where small V signals are detectable.

If the Ti (2p) peak contains a contribution from the metal below the surface oxide (information depth of XPS is about 6 nm in the case of TiO_2), the thickness of the oxide layer can be calculated. If one assumes this layer to be uniformly thick on a flat substrate, the expression to estimate the thickness, d, is [26]

$$d = \lambda_{TiO_2} \times \sin\phi \times \ln\left(\frac{I_{TiO_2}}{I_{Ti}} \times \frac{N^{\infty}_{Ti} \times \lambda^{\infty}_{Ti}}{N^{\infty}_{TiO_2} \times \lambda^{\infty}_{TiO_2}} + 1\right) \quad (1)$$

where ϕ is the electron take-off angle of the XPS (here 90°); $\lambda^{\infty}_{TiO_2}$ and λ^{∞}_{Ti} the mean free path of the electrons in the oxide layer and the substrate, respectively; I_{TiO_2} and I_{Ti} the measured Ti (2p) intensity due to the oxide layer of thickness, d, and the underlying metal, respectively; and N^{∞}_{Ti} and $N^{\infty}_{TiO_2}$ the atomic densities of the Ti atoms in the substrate and TiO_2 molecules in the oxide layer, respectively. Values for the mean free path are calculated as described by Briggs and Seah [26], resulting in $\lambda^{\infty}_{TiO_2} = 1.5$ nm and $\lambda^{\infty}_{Ti} = 1.7$ nm, which correspond well to values reported in the literature [27, 28].

3. Results

Because special emphasis was put on the statistical significance of the analytical results, five–six measurements were performed for each surface preparation type.

3.1. Microstructure and surface topography

Both the metallography (Fig. 1) and the SEM images of the polished alloys (Fig. 2) clearly show the expected duplex microstructure. Al stabilizes the low-temperature α-phase (hexagonal close packed, h.c.p.), while Nb (or V) stabilizes a small amount of the high-temperature β-phase (body-centred cubic, b.c.c.). The latter phase thus contains a higher concentration of Nb (or V), whereas Al is enriched in the α-phase. The resulting microstructure of these alloys can be described as grains consisting of pure α-phase surrounded by a mixture of α and small amounts of β. The α-grains are somewhat larger for the Ti–6Al–7Nb than for the Ti–6Al–4V alloy.

Pickled surfaces investigated by SEM show material-specific surface structures (Fig. 3). C.p. Ti is pickled irregularly. The pickling rate is dependent on grain orientation, thus leading to a rough surface topography and to pit formation (Fig. 3a). Ti–6Al–7Nb is selectively pickled with the α-phase dissolving at a higher rate. Therefore, the β-phases from ridges as illustrated in Fig. 3b with the β-phase appearing brighter because of the higher secondary electron emission. The pickled Ti–6Al–4V alloy also shows a topography reflecting its microstructure (Fig. 3c). Compared with Ti–6Al–7Nb, a finer topography is developed due to the finer microstructure and also possibly due to the pickling rate of the α- and β-phases corresponding more closely than in the case of the Nb-containing alloy.

R_a, $R_{z_{iso}}$ and N_r were determined by non-contact laser profilometry on the different surfaces (Table III). As expected, polished surfaces are much smoother than pickled ones for the three materials. To investigate specifically the influence of the type of material on the surface roughness, polished samples from each material were pickled under the same conditions (ultrasonically for 10 min). The results show that the pickled Ti–6Al–4V surfaces are smoother than the corresponding c.p. Ti or Ti–6Al–7Nb surfaces. The surface condition prior to pickling also influences the roughness values, as can be seen from differences arising between polished versus cold-worked plus annealed (for c.p. Ti), polished versus turned (for Ti–6Al–7Nb), and polished versus cut (for Ti–6Al–4V) samples. Furthermore, ultrasonic agitation also influences the roughness of c.p. Ti surfaces, but only when samples had been polished prior to pickling.

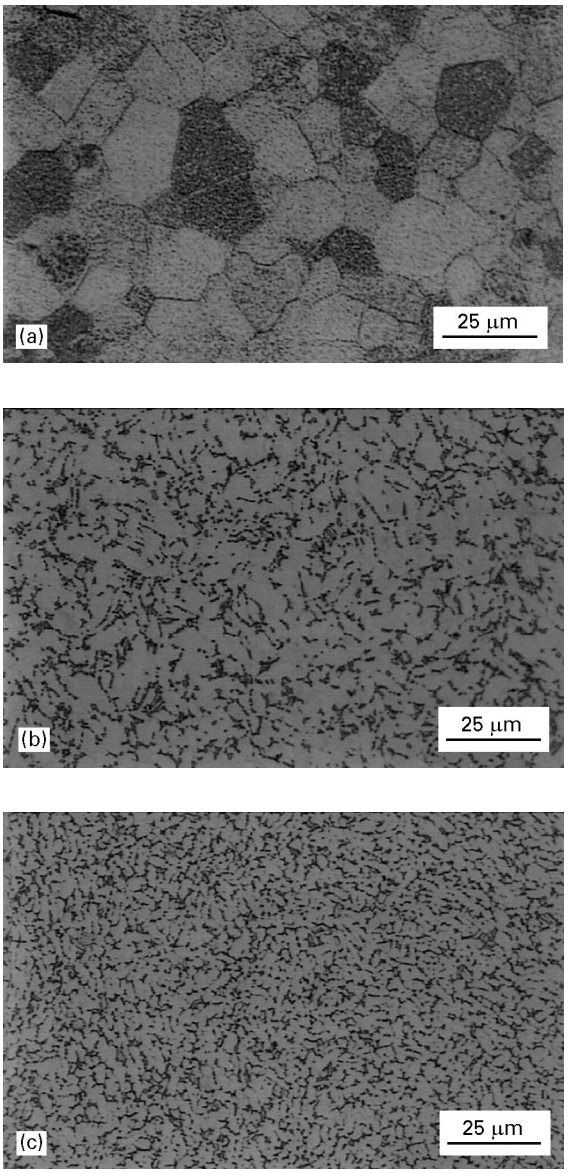

Figure 1 Metallographic analysis of (a) c.p. Ti, (b) Ti–6Al–7Nb, and (c) Ti–6Al–4V.

3.2. Chemical composition of the surface by XPS

The surface composition as determined by quantitative XPS and the measured binding energies for Ti, Al, Nb and V are given in Tables IV and V, respectively.

3.2.1. Commercially pure Ti

Fig. 4 shows a typical XPS survey spectra for a polished, passivated and pickled c.p. Ti surface, respectively. Ti, O, C and N are present on all surfaces. As expected, the spectra are dominated by Ti and O emission

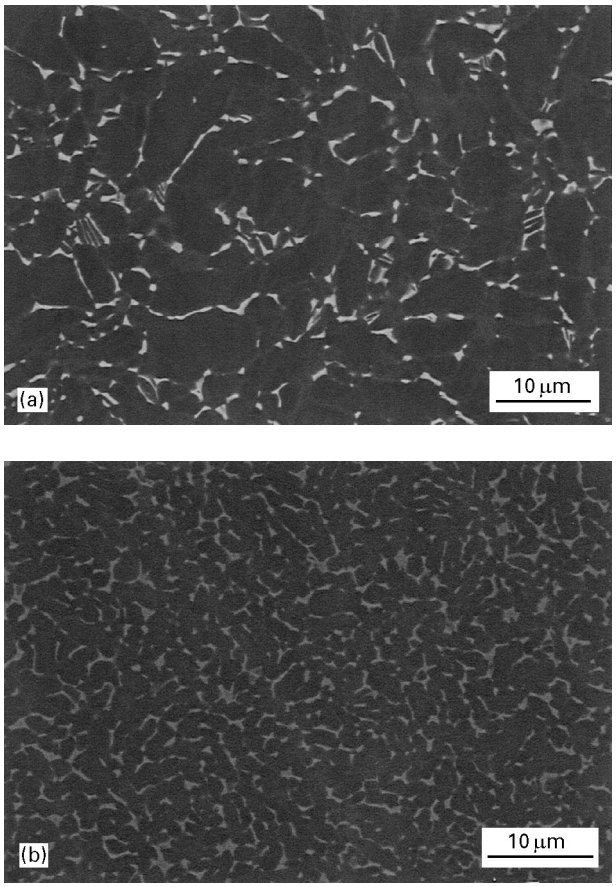

Figure 2 SEM images (composition contrast mode) of the polished alloys, Ti–6Al–7Nb (a), and Ti–6Al–4V (b).

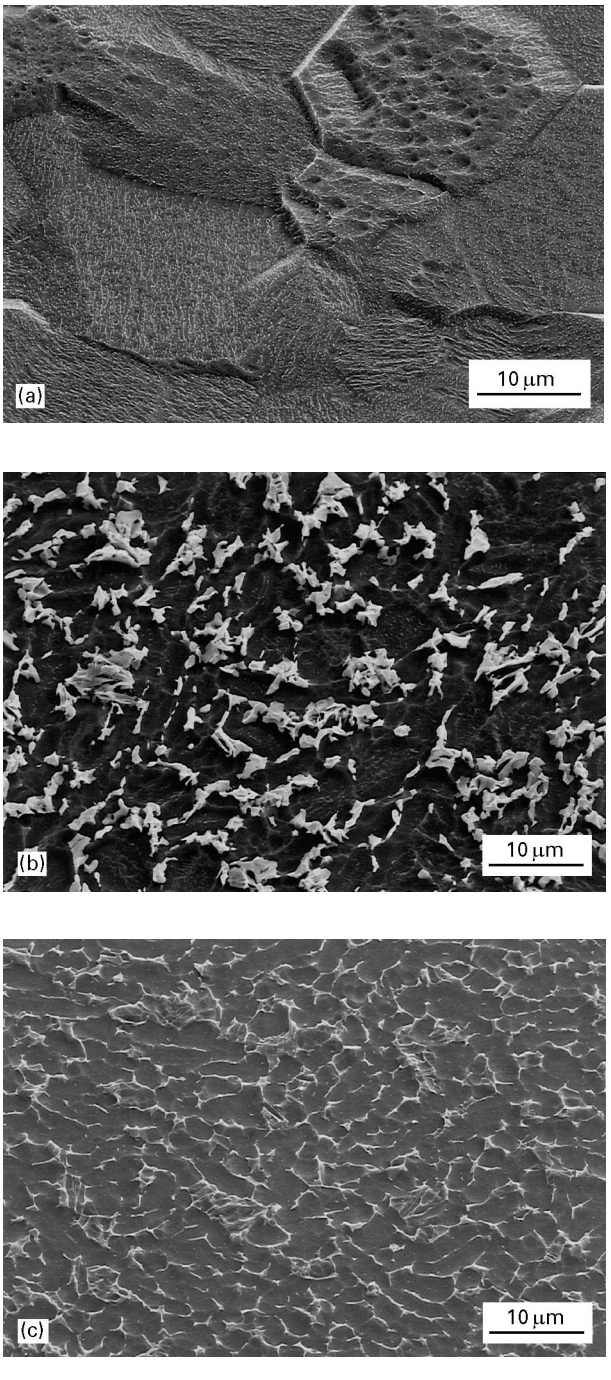

Figure 3 HNO_3–HF-pickled (10 min, with ultrasonic agitation) surfaces of (a) c.p.Ti, (b) Ti–6Al–7Nb, and (c) Ti–6Al–4V investigated by SEM.

intensities due to the naturally formed TiO_2 layer (see below). The relatively strong C signal is typical for adsorbed organic molecules and is always present on high surface area oxide films that have been exposed and stored under atmospheric conditions. On most of the surfaces, some contamination by Si (polydimethylsiloxane, as determined with time-of-flight secondary ion mass spectroscopy (ToF–SIMS); data not shown) was detected. The pickled surfaces showed the presence of F, Na, Ca, Cu and Zn contaminants.

3.2.2. Ti–6Al–7Nb

As in the case of c.p. Ti, the surface consists mainly of titanium oxide, but in addition the alloying elements are incorporated in the oxide film in their most stable oxidation states, i.e. Al_2O_3 and Nb_2O_5.

Traces of Ca, Si, Zn, Cu, P, Na, Pb and F were detected on the polished samples, whereas only Si, Ca and P were found on the passivated samples. It can be concluded that passivation by HNO_3 efficiently removed the contaminants Zn, Cu and Pb. On the pickled samples only traces of F, Na and Si were detected.

Fig. 5 compares the XPS surface concentrations (wt %) of Ti, Al, Nb with the bulk composition. On the polished and passivated samples the Al concentration is increased at the surface, while the concentration of Nb at the surface is similar to that in the bulk. The pickled Ti–6Al–7Nb samples show, on the other hand, a significantly higher amount of Nb at the surface.

Sterilization did not lead to a significant change of the surface composition (Table VI).

3.2.3. Ti–6Al–4V

Ti, Al, O, C and N are present on the surfaces of all samples. V was only detected when using monochromated excitation radiation (ϕ 5700). The surface is composed mainly of titanium oxide (TiO_2), with the addition of the alloying elements in oxidized form. Al is present as Al_2O_3, whereby the situation with V is less clear: the experimental binding energy is in a range where different oxidation states [V(III),

TABLE III Surface roughness parameters of differently prepared surfaces on c.p. Ti, Ti–6Al–7Nb and Ti–6Al–4V, measured with a non-contact laser profilometer

Material	Pretreatment	Pickling	Roughness values		
			R_a (μm)	$R_{z_{iso}}$ (μm)	N_r (cm^{-1})
Without pickling					
c.p. Ti	Polished or passivated	None	0.042 ± 0.004	0.72 ± 0.13	0 ± 0
Ti–6Al–7Nb	Polished or passivated	None	0.009 ± 0.001	0.14 ± 0.07	0 ± 0
Ti–6Al–4V	Polished or passivated	None	0.017 ± 0.002	0.14 ± 0.03	0 ± 0
Influence of the type of material on the surface roughness after pickling					
c.p. Ti	Polished	10 min[a]	0.52 ± 0.05	6.19 ± 0.56	209.1 ± 20.1
Ti–6Al–7Nb	Polished	10 min[a]	0.60 ± 0.04	5.74 ± 0.32	548.1 ± 35.1
Ti–6Al–4V	Polished	10 min[a]	0.36 ± 0.04	3.85 ± 0.35	287.4 ± 67.1
Cold-worked + annealed pickled versus polished pickled surfaces for c.p. Ti					
	Cold-worked + annealed	3 min[a]	1.02 ± 0.08	10.43 ± 1.07	522.7 ± 19.6
	Polished	3 min[a]	0.49 ± 0.08	5.80 ± 0.97	204.9 ± 31.3
Turned pickled versus polished pickled surfaces for Ti–6Al–7Nb					
	Turned	4 min[a]	1.25 ± 0.08	9.12 ± 0.88	349.0 ± 20.5
	Polished	10 min[a]	0.60 ± 0.04	5.74 ± 0.32	548.1 ± 35.1
Cut pickled versus polished pickled surfaces for Ti–6Al–4V					
	Cut	10 min[a]	0.59 ± 0.06	6.94 ± 0.71	290.3 ± 14.5
	Polished	10 min[a]	0.36 ± 0.04	3.85 ± 0.35	287.4 ± 67.1
Influence of ultrasonic agitation during pickling on c.p.Ti					
	Cold-worked + annealed	3 min[a]	1.02 ± 0.08	10.43 ± 1.07	522.7 ± 19.6
	Cold-worked + annealed	3 min	0.95 ± 0.03	9.39 ± 0.98	522.2 ± 25.1
	Polished	3 min[a]	0.49 ± 0.08	5.80 ± 0.97	204.9 ± 31.3
	Polished	3 min	0.24 ± 0.02	2.94 ± 0.54	94.5 ± 20.2

[a] With ultrasonic agitation during pickling.

TABLE IV XPS analysis[a]: quantitative surface compostion (at %) and oxide film thickness (nm), of c.p. Ti, Ti–6Al–7Nb and Ti–6Al–4V after different surface treatments

Element	c.p. Ti			Ti–6Al–7Nb			Ti–6Al–4V		
	Polished	Passivated	Pickled	Polished	Passivated	Pickled	Polished	Passivated	Pickled
Ti	19.2 ± 1.3	21.4 ± 1.3	17.9 ± 1.0	19.7 ± 0.4	21.5 ± 1.1	19.9 ± 0.6	13.8 ± 1.0	19.2 ± 1.4	17.2 ± 1.4
Al	–	–	–	3.6 ± 0.3	4.0 ± 0.5	2.2 ± 0.5	3.3 ± 0.6	2.6 ± 0.8	3.5 ± 0.3
Nb	–	–	–	0.7 ± 0.1	0.9 ± 0.1	3.3 ± 0.2	–	–	–
V	–	–	–	–	–	–	0.29 ± 0.06[b]	0.54 ± 0.04[b]	0.67 ± 0.05[b]
O	47.1 ± 1.9	49.9 ± 0.6	47.6 ± 1.2	53.4 ± 1.0	52.8 ± 2.9	58.1 ± 1.7	46.7 ± 1.6	50.9 ± 1.7	50.2 ± 3.1
C	30.6 ± 2.1	26.7 ± 0.9	29.2 ± 1.5	18.2 ± 1.0	18.6 ± 3.9	15.4 ± 2.7	30.2 ± 2.8	23.8 ± 2.2	26.8 ± 3.5
N	1.3 ± 0.5	1.1 ± 0.4	1.2 ± 0.4	0.6 ± 0.2	1.0 ± 0.4	0.4 ± 0.3	1.3 ± 0.5	1.2 ± 0.4	1.5 ± 0.3
Additionally detected elements	Si, Pb	Si	Si, Cu, Ca, F, Na, Zn	Si, Ca, P, Na, F, Zn, Pb	Si, Ca, P	F, Na	Si, Ca, Na, S, P, Zn	Si, S	Si, S
Relative oxide thickness	4.9 ± 0.1	4.9 ± 0.1	> 6	5.0 ± 0.1	4.7 ± 0.1	5.9 ± 0.1	4.8 ± 0.1	4.9 ± 0.2	> 6

[a] All values are mean values ± standard deviation; the samples were measured at least 50 days after polishing.
[b] Samples measured separately using monochromatized radiation (ϕ 5700), relative to Ti 2p signal, mean of four samples.

V(IV) and V(V)] have been reported in the literature [29]. The Al surface concentration is higher while the V concentration is lower at the surface as compared with the bulk (Fig. 6). Pickling increases the surface concentration of V above that of the polished sample.

3.2.4. Surface oxide stoichiometry

Fig. 7 shows a Ti 2p spectrum for the surface of a freshly polished Ti–6Al–7Nb sample. The dominant Ti (2p3/2) peak is at a binding energy of 459.1 eV and can be assigned to Ti (IV) (TiO_2). A small peak at 454.1 eV is typical for metallic Ti. The observed chemical shift between the oxide peak and the metal peak agrees well with the expected value for TiO_2 [27, 29, 30]. At the freshly polished surface a shoulder at 457.3 eV is clearly visible and can be assigned to Ti (III) (Ti_2O_3) [31, 32]. Small intensity contributions were generally observed near 455.7 eV and assigned to Ti (II) (TiO). Deconvolution of the Ti (2p) peak was

TABLE V Binding energies measured with XPS for Ti, Al, Nb and V

Element	Binding energy (eV)	Assigned chemical state
Ti (2p3/2)	459.1 ± 0.2	Ti (IV), TiO_2
	457.3 ± 0.3	Ti (III), Ti_2O_3
	455.7 ± 0.2	Ti (II), TiO
	454.1 ± 0.2	Ti (metallic)
Al (2p)	74.8 ± 0.3	Al_2O_3
Nb (3d)	207.8 ± 0.1	Nb_2O_5
V (2p)	516.4 ± 0.4	V-oxide

systematically carried out, based on the components listed in Table V. Whether the lower valence states Ti (III) and Ti (II) are due to defined suboxide phases or to non-stoichiometric defect states of the TiO_2 cannot be determined from XPS measurements.

3.2.5. Oxide film thickness

Using Equation 1 (Section 2.3.), values between 4 and 6 nm were found for the thicknesses of the oxide layers of polished and passivated samples with a native oxide layer (Table IV). The reproducibility of the oxide thickness calculation from XPS Ti (2p) spectra is typically ± 0.1 nm, but the absolute thickness is not known exactly. The pickled samples show a slightly larger oxide layer thickness (between 5 and > 6 nm). This is probably an artefact due to the increased roughness of this surface.

The oxide layer thickness also depends on the time of exposure to air, as shown in Fig. 8. The evolution of the oxide film thickness on polished c.p. Ti and Ti–6Al–7Nb complies with the generic logarithmic equation due to Uhlig [33] (Fig. 8), which gives typical rates for the formation of thin passive layers on metals. There is no significant difference between the two materials c.p. Ti and Ti–6Al–7Nb in this respect.

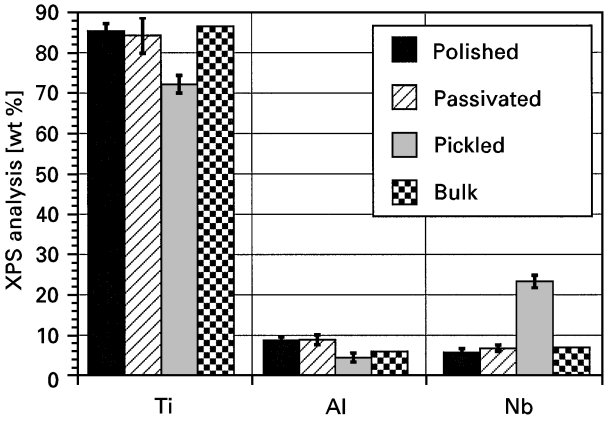

Figure 5 Ti–6Al–7Nb alloy composition at the surface (XPS data converted to weight percent, normalized to Ti + Al + Nb = 100 wt %) compared with the bulk composition.

4. Discussion

4.1. Topography

Different mechanical and chemical surface pretreatment processes, all of relevance to the manufacturing of titanium implants, have been studied and their effect on surface topography investigated using non-contact laser profilometry and SEM.

4.1.1. Polished surfaces

Polished surfaces with R_a and $R_{z_{iso}}$ parameters down to 0.01 and 0.14 μm, respectively, can be produced, at which point the z-resolution limit of the laser

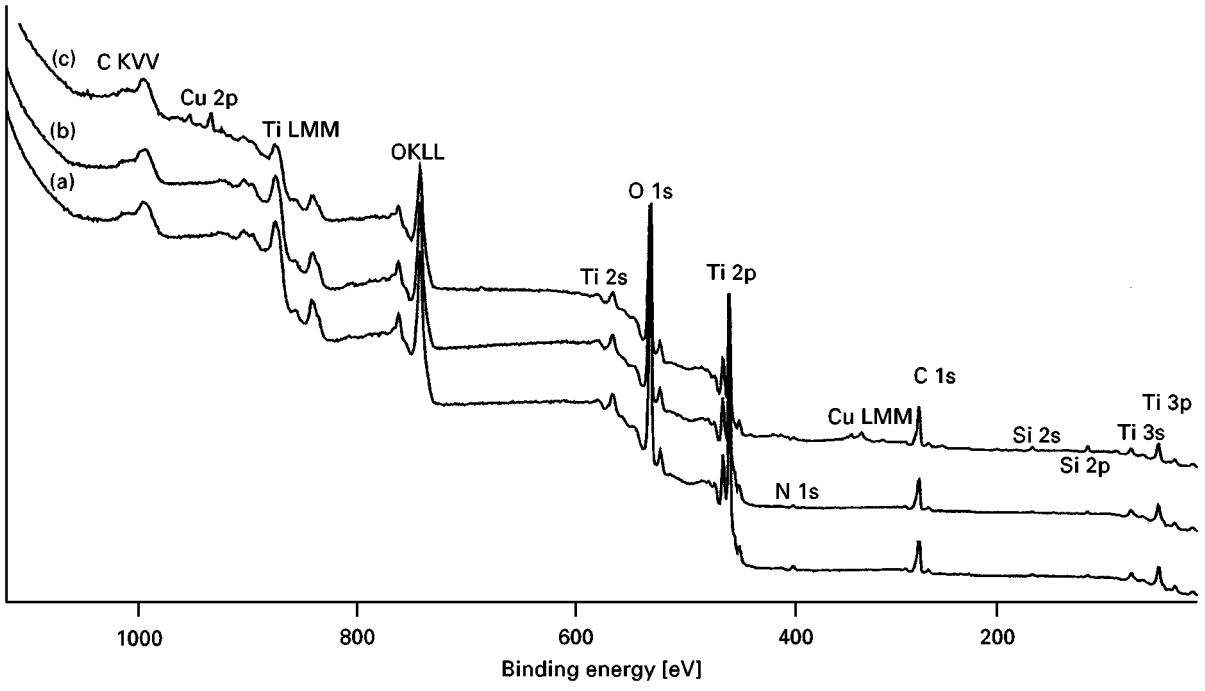

Figure 4 Typical XPS survey spectra for (a) a polished, (b) a HNO_3-passivated, and (c) a HNO_3–HF-pickled c.p. Ti surface.

TABLE VI XPS analysis (at %) of Ti–6Al–7Nb unsterilized and sterilized sample surfaces

	Polished	Polished sterile	Passivated	Passivated sterile	Pickled	Pickled sterile
Ti	19.7 ± 0.4	16.5 ± 0.9	21.5 ± 1.1	19.6 ± 3.0	19.9 ± 0.6	19.2 ± 0.8
Al	3.6 ± 0.3	4.4 ± 0.9	4.0 ± 0.5	3.6 ± 0.4	2.2 ± 0.5	2.7 ± 0.1
Nb	0.7 ± 0.1	0.5 ± 0.1	0.9 ± 0.1	0.7 ± 0.1	3.3 ± 0.2	3.2 ± 0.2
O	53.4 ± 1.0	49.0 ± 1.7	52.8 ± 2.9	51.0 ± 4.6	58.1 ± 1.7	56.0 ± 1.2
C	18.2 ± 1.0	24.1 ± 3.7	18.6 ± 3.9	22.2 ± 7.3	15.4 ± 2.7	17.2 ± 1.6
N	0.6 ± 0.2	1.1 ± 0.5	1.0 ± 0.4	1.7 ± 0.7	0.4 ± 0.3	0.6 ± 0.2
Additional detected elements	Si, Ca, P, Na, F, Zn, Pb	Si, Ca, P, Cu, F, Na, Zn	Si, Ca, P	Si, Ca, F	F, Na	F, Si

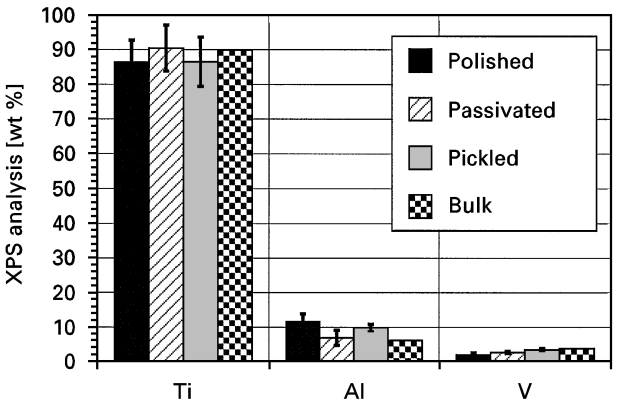

Figure 6 Ti–6Al–4V alloy elemental surface concentration (XPS data converted to weight percent normalized to Ti + Al + V = 100 wt %) compared with the bulk composition.

profilometer is reached. For comparison, atomic force microscopy (AFM, Nanoscope III, Digital Instruments) performed on the same samples gave R_a values between 1 and 3 nm (on a measured area of $10 \times 10\ \mu m^2$).

4.1.2. Passivation

Nitric acid treatment turned out to have no significant effect on surface roughness parameters, because the dissolution rate was obviously very low for both the α- and the β-phases present in the alloys. Neither the α- nor the β-phase was preferentially attacked.

4.1.3. Pickling of c.p. Ti in HNO_3–HF

C.p. Ti develops a surface topography that is due to locally different pickling rates on grains and subgrains of different orientation (Fig. 9) and in addition shows some pitting attack. The result is a "relatively smooth" surface. This characteristic surface structure develops within a few (up to three) minutes, after which surface roughness values do not show significant further changes with time (compare 3 and 10 min pickling times, Table III). It is believed that after the initiation stage, during which preferential surface sites are attacked, the fairly high hydrodynamic regime created by ultrasonic agitation induces a very thin diffusion layer that follows the surface topography. In such a case (often called macroprofile), the diffusion rate is equal over

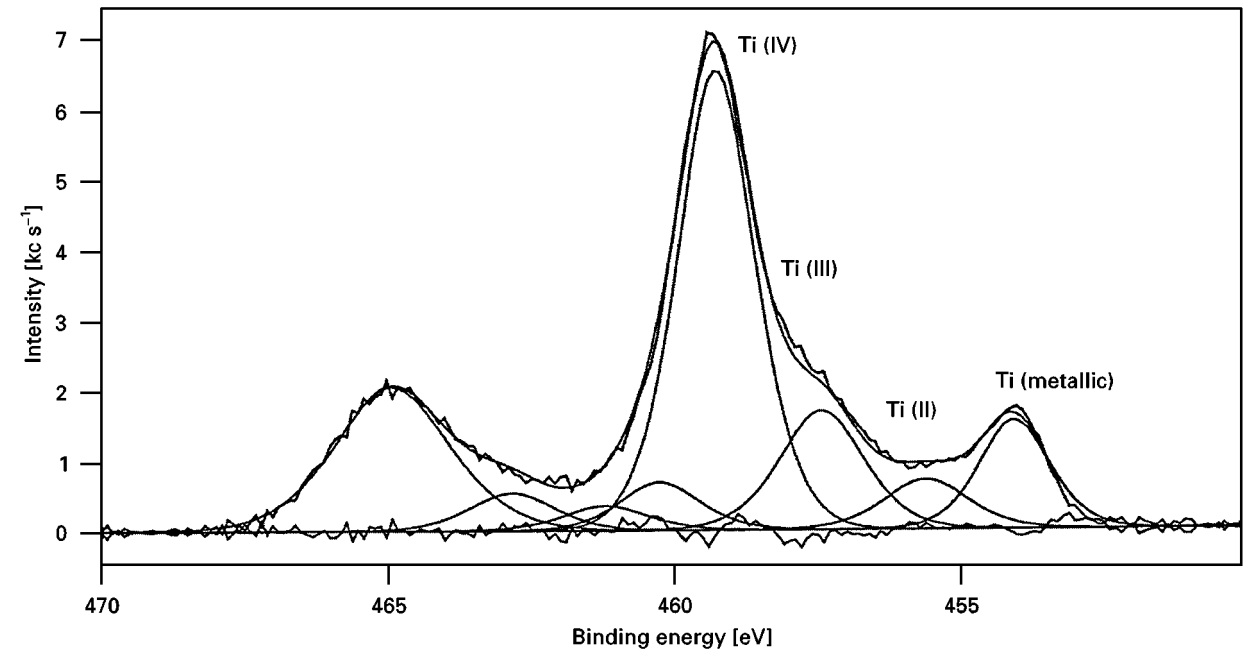

Figure 7 Ti 2p XPS spectrum of a freshly polished Ti–6Al–7Nb surface.

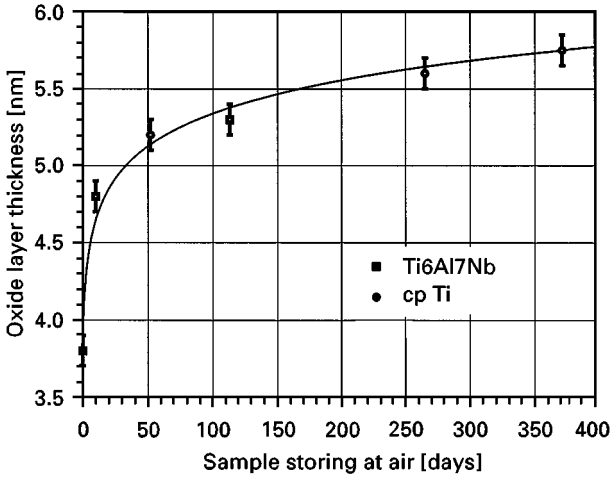

Figure 8 The evolution of the oxide film thickness on polished c.p. Ti (●) and Ti–6Al–7Nb (■) dependent of storing time. The curve shown corresponds to a least-square fit based on a logarithmic rate law [with $y = 0.313 \times \ln(24\,900 \times x + 1)$].

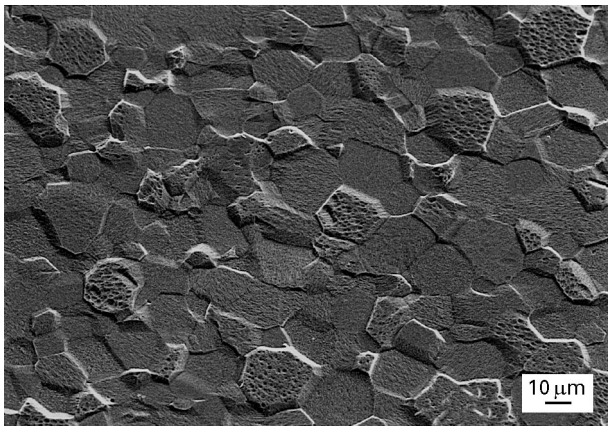

Figure 9 SEM image of a HNO_3–HF-pickled (10 min with ultrasonic agitation) c.p. Ti surface.

the whole surface and dissolution proceeds homogeneously over the entire topography, maintaining the aspect ratio between "peaks" and "valleys". On surfaces polished prior to pickling, the use of ultrasonic agitation during pickling increases the surface roughness at short treatment times (3 min, c.p. Ti). In this case, ultrasonic agitation is believed to initiate chemical attack more rapidly by removing contaminants remaining after the polishing procedure more quickly. No significant effect of ultrasonic action could be seen on cold-worked plus annealed c.p. Ti surfaces.

4.1.4. Pickling on Ti alloys

The effect of the microstructure of the alloy on the surface topography after pickling has to be emphasized. Although Ti–6Al–7Nb shows the same R_a and $R_{z_{iso}}$ values as c.p. Ti after 10 min pickling on polished surfaces, a large difference in the N_r values (number of peaks) is observed, suggesting very different surface structures in the two cases. SEM demonstrates that the two alloys develop a surface topography during pickling depending on their specific microstructure

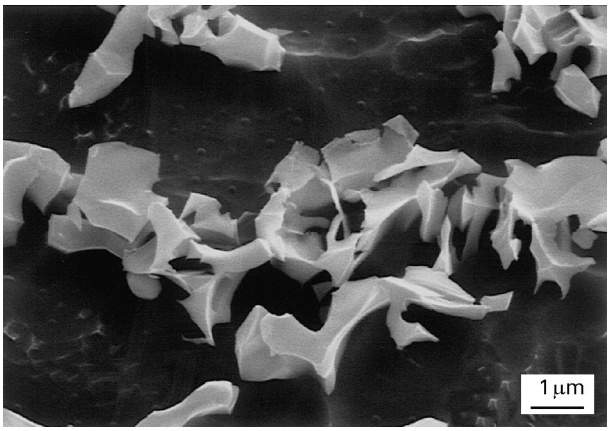

Figure 10 SEM image of a HNO_3–HF-pickled (10 min with ultrasonic agitation) Ti–6Al–7Nb surface.

and metallurgical phase reactivity. In both alloys the β-phase is less rapidly attacked by the HNO_3–HF acid bath and in the course of the pickling process forms ridges. The α-phase, on the other hand, is preferentially attacked, particularly in areas close to β-segregation. This is thought to be an effect of electrochemical potential differences, with the α-phase being more anodic compared with the β-phase. The roughness that develops during pickling is dependent on the relative dissolution rate of the two metallurgical phases present and on the average size of the β-phase.

The two alloys show subtle differences in their pickling response, however. The Nb-containing β-phase clearly has very low solubility in the pickling solution and remains almost unattacked on the surface, forming very sharp ridges (Fig. 10). The V-containing β-phase, on the other hand, shows a dissolution rate that is more comparable with that of the α-phase. Together with the fact that the microstructure is finer for the V alloy, it is therefore understandable that the roughness level that develops on the V alloy is lower than that on the Nb alloy.

In order to relate the SEM observations to the XPS results, the SEM pictures were quantitatively evaluated using an image analyser. Table VII shows the comparison of the relative ratios of the β-phase to the total area and the corresponding XPS ratios. Although a quantitative relationship cannot be expected, both methods show the same trend, i.e. a relative increase in the proportion of the β-phase at the surface following HNO_3–HF pickling.

4.2. Chemical composition of the surface

The composition of the protective oxide film, relevant for both corrosion resistance and biological properties, turns out to depend on both the bulk alloy composition and surface-treatment procedures.

4.2.1. Oxide film thickness

When stored under normal ambient conditions, the thickness of the oxide film slowly increases with time, approaching 6 nm after one year, for both c.p. Ti and

TABLE VII Ratio of Nb/Ti or V/Ti from XPS and relative fraction of $\beta/(\alpha+\beta)$-phase (image analyser) on polished and pickled (10 min with ultrasonic treatment) surfaces, respectively

Alloy	Surface treatment	XPS ratio Nb (V)/Ti (at %/at %)	SEM $\beta/(\alpha+\beta)$-phase (area/area)
Ti–6Al–7Nb			
	Polished	0.03 ± 0.01	0.08 ± 0.02
	Pickled	0.13 ± 0.05	0.28 ± 0.06
Ti–6Al–4V			
	Polished	0.02 ± 0.01	0.10 ± 0.02
	Pickled	0.03 ± 0.01	0.14 ± 0.03

Ti–6Al–7Nb (Fig. 8). The logarithmic rate law, which fits well with the experimental data, is typical for field-assisted growth of thin passive layers on metals.

4.2.2. Oxide film stoichiometry

The predominant oxidation state in the oxide film of c.p. Ti and the two alloys is Ti (IV) (TiO_2), in agreement with XPS measurements on TiO_2 standards and literature on titanium surface films [29, 32, 34]. In addition, smaller proportions of Ti (III) and Ti (II) are present, as found in several other XPS studies [30–32, 35]. Whether these are distinct phases or non-stoichiometric defect states cannot be decided from XPS measurements. Angle-dependent measurements (ϕ 5700, Fig. 11) imply the presence of a "gradiated stoichiometry", with a gradient Ti (IV)–Ti (III)–Ti (II)–Ti (0, metal), as one moves from the oxide–air interface to the metal substrate. Passivation with nitric acid does not change the overall thickness of the oxide film. The assumption is that HNO_3 could improve the homogeneity of the passive film at local defects (flaws, voids, etc.); this, however, cannot be detected by XPS.

4.2.3. Oxides on alloys

All alloying elements, i.e. Al, Nb and V, are found to be present in the oxide film in oxidized form (Al_2O_3, Nb_2O_5). The oxidation state(s) of V could not be unambiguously assigned. If one compares the XPS-derived oxide-film composition on polished and HNO_3-passivated surfaces with the bulk analysis (Figs 5 and 6), some subtle differences are noted: Al is present in the oxide film in higher concentration, Nb is present in approximately the same concentration and V is present in lower concentration compared with the bulk composition. The main observed change (Fig. 5) is the increase of Nb in Ti–6Al–7Nb alloy after HNO_3–HF pickling, which confirms the selective pickling pattern also observed by SEM and in the topography measurements (Section 4.1.). It is assumed that the composition of the oxide film above α- and β-phases reflects the local composition of the phases with Al-rich α- and Nb- or V-rich β-phases, respectively. Indeed, a preliminary study using scanning Auger microscopy with submicrometre lateral resolution capability has shown a distribution of Ti, Al and Nb

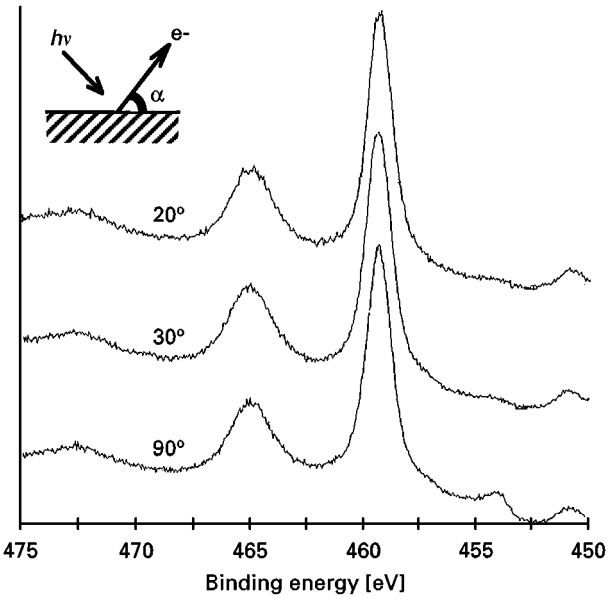

Figure 11 Angle-dependent XPS measurements of Ti 2p signal.

reflecting the bulk microstructure [36]. γ-sterilization under industrial conditions does not significantly affect the surface composition of the different sample surfaces studied (Table VI). Although the average carbon surface concentration determined by XPS turns out to be always higher after sterilization, the differences are not really significant in view of the relatively high standard deviations of the carbon surface concentration (in fact much higher than for the other oxide film elements).

4.2.4. Surface contamination

The titanium oxide surface has a high tendency to react with both inorganic and organic contaminants from air or aqueous solutions. This study shows that the passivation treatment with HNO_3 is efficient in removing transition metals such as Cu, Zn and Pb, which could have a detrimental effect on the biological performance of titanium surfaces.

4.3. Biological relevance

Our experimental findings regarding the physico-chemical properties of titanium and its alloys are believed to be of significance with respect to some biocompatibility issues in connection with the use of these materials in implants.

Our study shows that a topography with a characteristic structure and roughness in the micrometre range can be generated by HNO_3–HF pickling. In the case of c.p. Ti, the topography of the pickled surface is directly dependent on the microstructure, due to preferential crystallographic attack. Because the microstructure depends, in turn, on earlier thermo-mechanical treatments of the material, it may be possible to obtain regular, size-controlled surface protrusions, reproducing directly the underlying recrystallized grain structure. One can, for instance, imagine using this technique for fabrication of model

surfaces for biocompatibility–cell culture studies: topographies of different dimensions could be fabricated and tested for their ability to accommodate cells of different sizes.

In the case of the alloys, the surface structure after pickling is mostly given by the protruding secondary phases and is therefore again dependent on the microstructure. However, on Ti–6Al–7Nb in contrast to c.p. Ti, very sharp β-phase surface features are formed (Fig. 10), which could be of potential harm to attached cells under mechanical shear forces.

Whether the pickling process could be used also for the fabrication of implant surfaces is, on the other hand, more difficult to assess, because both surface topography and mechanical properties have to be taken into account. Both properties (which are of major importance for implant applications) are directly related to the microstructure and cannot be independently optimized with pickling. For that purpose, it might be more convenient to obtain specific topographies by using other structuring methods that are not directly dependent on the microstructure. As an example, c.p. Ti surfaces treated with a combination of sandblasting and etching (with no preferential crystallographic attack) have already shown excellent biological performance *in vitro* [21, 22].

The surface composition of Ti–6Al–7Nb and Ti–6Al–4V has been shown to differ from that of c.p. Ti. The local presence of the alloying elements Al, V and Nb within the passive oxide film is likely to influence the adsorption of proteins and their conformation on the surface, which is in turn expected to modify surface–cell interaction. One property influencing interaction with proteins is the isoelectric point (IEP) of the surface: the IEP of TiO_2 is reported to be in the range 5 to 7 [37, 38]. It is certainly modified by the presence of Al (the IEP of Al_2O_3 is about 8), Nb (the IEP of Nb_2O_5 is about 4.5) or V (the IEP of V_2O_5 is between 1 and 2.5) [38]. The results of the surface charge measurements will be reported separately.

The surface composition also determines the corrosion properties. This is important to note with regard to potential tissue reactions that could be induced by corrosion products when the material is exposed *in vivo* to quite aggressive biological fluids. Ionic corrosion species are known to be more critical, due to their affinity for strong interactions with biological molecules. Whereas c.p. Ti shows mainly neutral species at pH 7 [$Ti(OH)_4$] with very low concentrations of ionic species ($< 10^{-12}$ M), the presence of other elements in the alloys could be suspected of inducing corrosion products that can initiate adverse cell reactions. This is particularly true for V, for which negatively charged corrosion species dominate [1, 4]. However, this study shows that the presence of V in the surface oxide film is strongly reduced in comparison with the bulk composition (Table IV, Fig. 6). This could explain why for instance, *in vivo* push-out studies did not reveal significant differences between c.p. Ti, Ti–6Al–4V and Ti–6Al–7Nb [23] and more generally why Ti–6Al–4V is still a widely used alloy for biomedical applications.

5. Conclusions

The composition of the 4–6 nm thick, native oxide film depends on the mechanical and chemical pretreatment of the surface.

For c.p. Ti the oxide film is predominantly TiO_2 with minor amounts of Ti (III) and Ti (II) oxidation states close to the oxide–metal interface.

Oxide films on the alloys Ti–6Al–7Nb and Ti–6Al–4V, naturally grown at room temperature, contain the alloying elements in oxidized form. On mechanically polished surfaces, aluminium in the oxide film is enriched compared to the bulk concentration, niobium is present approximately at the same level and vanadium is strongly depleted. It is expected that the presence of the alloying elements in the oxide layer influence the reactions between the implant surface and the biological environment.

Nitric acid–hydrofluoric pickling causes a roughening of the surface due to material dependent dissolution mechanisms: grain-orientation-dependent etch rates in the case of c.p. Ti and selective α-phase dissolution and β-phase precipitate enrichment in the cases of the α–β alloys Ti–6Al–7Nb and Ti–6Al–4V. The relevance of the resulting surface morphologies for surface–cell interactions has been discussed. In view of the possibility of adjusting the microstructure of these materials through specific thermo-mechanical treatment, model surfaces with controlled topographical variations could be fabricated for biocompatibility–cell culture studies.

Acknowledgements

The authors would like to thank Mr M. Windler of Sulzer Orthopedics Ltd, CH-8404 Winterthur, for technical support and supply of materials; Mrs D. Müller and Mr P. Habersetzer of Institut Straumann AG, CH-4437 Waldenburg, for sample preparation; and Mrs B. Wessicken and Mr W. Hotz of Alusuisse Technology & Management AG, CH-8212 Neuhausen, for the SEM measurements and imaging analysis.

References

1. S. G. STEINEMANN and P. -A. MÄUSLI, in Proceedings of the Sixth World Conference on Titanium, Cannes, France, June 1988. Edited by P. Lacombe, R. Tricot and G. Beranger (1989) p. 535.
2. J. LAUSMAA, L. MATTSSON, U. ROLANDER and B. KASEMO, *Biomedical Mater.* Materials Research Society Symposia Proceedings, Vol. 55, edited by J. M. Williams, M. F. Nichols and W. Zingg (1986) 351.
3. B. KASEMO and J. LAUSMAA, *CRC Crit. Rev. Biocompat.* **4** (1986) 335.
4. S. G. STEINEMANN, in Proceedings of the Fifth International Conference on Titanium, Munich 1984, Vol. 2 (1985) p. 1373.
5. G. MEACHIM and R. B. PEDLEY, in "CRC fundamental aspects of biocompatibility", Vol. 1, edited by D. F. Williams (CRC Press, Boca Raton, FL, 1981) p. 107.
6. K. -M. HOLGERS, G. ROUPE A. TJELLSTRÖM and L. M. BJURSTEN, in Third International Conference on Biointeractions, Oxford, August (1990) p. 31.
7. B. D. RATNER, in "Surface characterization of biomaterials" (Elsevier Science, B.V., Amsterdam, 1988) p. 13.

8. T. ALBREKTSSON, P. -I. BRANEMARK, H. -A. HANSSON and J. LINDSTRÖM, *Acta Orthop. Scand.* **52** (1981) 155.
9. J. LAUSMAA, M. ASK, U. ROLANDER and B. KASEMO, *Mater. Res. Soc. Symp. Proc.* **110** (1989) 647.
10. P. TENGVALL and I. LUNDSTRÖM, *Clin. Mater.* **9** (1992) 115.
11. L. VROMAN and A. L. ADAMS, in "Proteins at interfaces, physicochemical and biochemical studies", edited by J. L. Brash and T. A. Horbett (American Ceramic Society Washington, DC, 1987) p. 154.
12. T. A. HORBETT and J. L. BRASH, *ibid.* p. 1.
13. A. P. AMEEN, R. D. SHORT, R. JOHNS and G. SCHWACH, *Clin. Oral Impl. Res.* **4** (1993) 144.
14. A. ARYS, C. PHILIPPART, N. DOUROV, Y. HE, Q. T. LE and J. J. PIREAUX, *J. Biomed. Mat. Res., Appl. Biomater.* (1998) in press.
15. H. -J. WILKE, L. CLAES and S. STEINEMANN, in "Clinical implant materials: advances in biomaterials", edited by G. Heimke, U. Sottész and A. J. C. Lee, Vol. 9 (Elsevier Science, B.V., Amsterdam, 1990) p. 309.
16. S. G. STEINEMANN, J. EULENBERGER, P. -A. MÄUSLI and A. SCHROEDER, in "Biological and biomechanical performance of biomaterials", edited by P. Christel, A. Meunier and A. J. C. Lee (Amsterdam, 1986) p. 409.
17. D. BUSER, R. K. SCHENK, S. STEINEMANN, J. P. FIORELLINI, C. H. FOX and H. STICH, *J. Biomed. Mater. Res.* **25** (1991) 889.
18. B. CHEHROUDI, T. R. L. GOULD and D. M. BRUNETTE, *ibid.* **24** (1990) 1203.
19. D. M. BRUNETTE, *Int. J. Oral Maxillofac. Impl.* **3** (1988) 231.
20. B. D. BOYAN, T. W. HUMMERT, D. D. DEAN and Z. SCHWARTZ, *Biomaterials* **17** (1996) 137.
21. Z. SCHWARTZ, J. Y. MARTIN, D. D. DEAN, J. SIMPSON, D. L. COCHRAN and B. D. BOYAN, *J. Biomed. Mater. Res.* **30** (1996) 145.
22. J. Y. MARTIN, Z. SCHWARTZ, T. W. HUMMERT, D. M. SCHRAUB, J. SIMPSON Jr, J. LANKFORD, D. D. DEAN, D. L. COCHRAN and B. D. BOYAN, *ibid.* **29** (1995) 389.
23. M. WONG, J. EULENBERGER, R. SCHENK and E. HUNZIKER, *ibid.* **29** (1995) 1567.
24. P. F. A. BIJLMER, *Metal Finishing* **68** (1970) 64.
25. S. EVANS, R. G. PRITCHARD and J. M. THOMAS, *J. Electron Spectrosc. Relat. Phenom.* **14** (1978) 341.
26. D. BRIGGS and M. P. SEAH, "Practical surface analysis", Vol. 1 (Wiley, Chichester, 1990) p. 210.
27. J. LAUSMAA, B. KASEMO and H. MATTSSON, *Appl. Surf. Sci.* **44** (1990) 133.
28. L. PORTE, M. DEMOSTHENOUS and TRAN MINH DUC, *J. Less-Common Met.* **56** (1977) 183.
29. J. F. MOULDER, W. F. STICKLE, P. E. SOBOL, K. D. BOMBEN and J. CHASTAIN "Handbook of X-ray photoelectron spectroscopy" (Perkin-Elmer Corporation, Physical Electronics Division, MN, 1992) p. 240.
30. A. F. CARLEY, P. R. CHALKER, J. C. RIVIERE and M. W. ROBERTS, *J. Chem. Soc. Faraday Trans. 1* **83** (1987) 351.
31. R. N. S. SODHI, A. WENINGER, J. E. DAVIES and K. SREENIVAS, *J. Vac. Sci. Technol.* **A9** (1991) 1329. Errata *J. Vac. Sci. Technol. A* **12** (1994) 267.
32. B. W. CALLEN, B. F. LOWENBERG, S. LUGOWSKI, R. N. S. SODHI and J. E. DAVIES, *J. Biomed. Mater. Res.* **29** (1995) 279.
33. H. H. UHLIG, *Corros. Sci.* **7** (1967) 325.
34. G. N. RAIKAR, J. C. GREGORY, J. L. ONG, L. C. LUCAS, J. E. LEMONS, D. KAWAHARA and M. NAKAMURA *J. Vac. Sci. Technol.* **A13** (1995) 2633.
35. K. E. HEALY and P. DUCHEYNE, *Biomaterials* **13** (1992) 553.
36. C. SITTIG, G. HÄHNER, A. MARTI, R. HAUERT, M. TEXTOR and N. D. SPENCER, in preparation.
37. G. D. PARFITT, *Prog. Surf. Membrane Sci.* **11** (1976) 181.
38. G. A. PARKS, *Chem. Rev.* **65** (1965) 177.

Received 4 September 1997
and accepted 26 January 1998